MATCH
Communications in Mathematical and in Computer Chemistry

MATCH Commun. Math. Comput. Chem. **97** (2027) 429–462
ISSN: 0340–6253
doi: 10.46793/match.97-2.02126

Hydrogenolysis of Xylitol to Value Added Products: A Mathematical Approach

Thandokuhle Quinton Ndlovu[a], Fernando P. da Costa[b], Vusi Mpendulo Magagula[a,c], Mzamo L. Shozi[a,*]

[a] *University of KwaZulu-Natal, South Africa*
[b] *Universidade Aberta and Center for Mathematical Sciences, Universidade de Lisboa, Portugal*
[c] *University of Eswatini, Eswatini*
ndlovuquinton4@gmail.com, fernando.costa@uab.pt, magagulav@ukzn.ac.za, shozim2@ukzn.ac.za

(Received January 20, 2026)

Abstract

In this paper we mathematically investigate the kinetics underlying the hydrogenolysis of xylitol over a metal based catalyst by using ordinary differential equations. The primary motivation for mathematically investigating this reaction lies on the fact that some of the value added products from this reaction are sourced from fossil fuels, which are not environmentally friendly. They have been reported by different researchers that they are the primary drive of global warming which leads to climate change, which causes severe disturbances in the Earth´s natural systems and economies. Xylitol, on the other hand, which is readily available from biomass have been reported as an alternative raw material for some of the value added products. A reaction mechanism proposed from experimental data is used to formulate a system of ordinary differential equations which is then analyzed using some qualitative analysis tools from mathematics.

*Corresponding author.

Numerical simulations are performed to try and ascertain the long time behavior of the system's solutions. Results showed that the solutions to the system approaches a lower dimensional invariant set with $X_k = 0$ for $k = 1, 2, ...8$ and $X_k > 0$ for $k = 9, 10, 11$. These numerical results were found to be in agreement with the experimental results from the chemistry point of view. Therefore, it is believed that this model can be extended for use in other sugar alcohols higher than xylitol, like sorbitol as means to maximize the yields of the desired products.

1 Introduction

The chemical industry has been using fossil fuels as the main resource since the end of the 18^{th} century´s Industrial revolution [5]. This has resulted in an increase in the consumption of oil by the chemical industry, with an approximation of over 1 billion barrels per year [1]. Consequently, this increase in oil consumption means an exponential growth in the amounts of carbon dioxide emissions, having reached 37.55 billion tons in 2023 [13]. This is a cause for concern, since high emissions of carbon dioxide contribute massively to climate change, which in turn causes many risks to human life and any other forms of life on Earth [6].

To counter these environmental impacts brought by the use of fossil fuels, alternative resources that are sustainable and environmentally friendly have become a priority in the chemical industry and are being studied extensively [6]. As a result, renewable resources such as lignocellulose, sugars and sugar alcohols have been increasingly of interest to researchers [18]. Research has shown that glycols, mainly ethylene glycol (EG) and propylene glycol (PG), are highly valued chemicals and very important intermediates in the chemical industry with different uses [2]. They are used in polymer chemistry, pharmaceutical industry, cosmetics, hydraulic brake fluids and as heat transfer liquids [9]. PG is a very excellent carrier for dyes, anti oxidants and enzymes while EG is mostly used as an anti-freezing agent in the aviation industry [19].

These wide industrial applications of EG and PG have resulted into an increase in their demand as a result they are being produced in higher

quantities (EG approximately 57 million tonnes in 2022 [12] and PG approximately 2 million tonnes in 2023 [14]). This means that environmentally friendly sources other than fossil fuels are to be considered. Therefore, the production of EG and PG from renewable biomass could play a vital role in this growing demand [10]. As a result, studies on the conversion of xylitol, a renewable source to valuable products such as EG and PG have become of great interest [15].

In this study we look at a reaction mechanism proposed by [15] on the hydrogenolysis of xylitol over nickel (Ni) catalysts supported on aluminium oxide (Al_2O_3) and magnesium oxide (MgO). From the mechanism, a kinetic model is developed and then validated with experimental data. It is then investigated and analyzed using qualitative techniques from ordinary differential equations. The result may be helpful in understanding the dynamics of the reaction so that optimization strategies may be proposed as means to develop and improve the reaction.

Although the study prioritizes heterogeneous catalytic pathways, it acknowledges the exclusion of other routes, like the enzymatic and non-catalytic routes. Therefore, the formulated model does not explicitly incorporate catalysts, temperature and mass transfer kinetics despite their known role in hydrogenolysis reactions.

2 Fundamentals

2.1 The mathematical approach

Most studies on xylitol hydrogenolysis have highlighted some gaps in their findings due to many factors. One of them is that the xylitol hydrogenolysis reaction is a very complex process because it is characterized by many reaction steps and a plethora of side products [10] which is a concern. As a result, there is a need for a more predictive model which will help scale down experimental trials and in the process help maximize the yields of desired products and subsequently improve the reaction. Therefore ordinary differential equations alongside qualitative analysis tools are used

to formulate and analyze the model.

2.2 Proposed reaction pathway

The reaction involves the use of a metal catalyst where xylitol and hydrogen gets adsorbed on the catalyst´s reaction sites. Once adsorbed, they react, generating a plethora of products while reforming the catalyst [15]. It has been proposed that the hydrogenolysis of polyols involves two key steps; i.e dehydrogenation of polyols to their corresponding carbonyl intermediates, followed by their C-C cleavage in the presence of bases [17]. Figure 1 illustrates the proposed mechanistic pathways for the reaction.

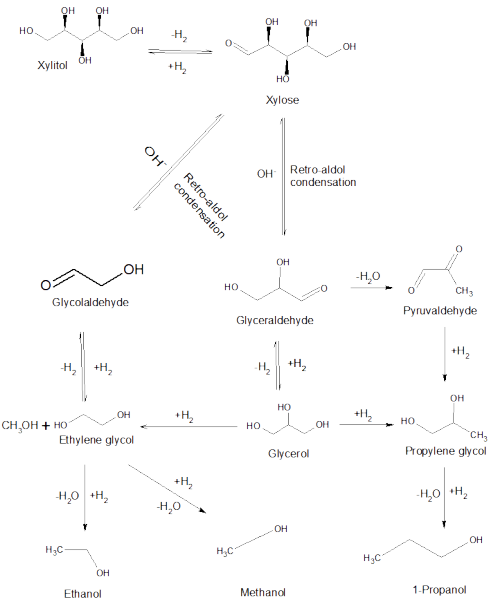

Figure 1. The proposed reaction pathways on hydrogenolysis of xylitol [15]

In the reaction scheme proposed by [15], the reaction begins by the dehydrogenation of xylitol to the corresponding xylose intermediate on the metal catalyst and at the same time, xylose is hydrogenated back to xylitol. Then, xylose undergoes retro-aldol condensation to form glycolaldehyde and glyceraldehyde, which can reform xylose in the presence of a base

(OH^-) as illustrated in Figure 1.

The formed glycolaldehyde is hydrogenated to ethylene glycol, which also undergo dehydrogenation back to glycolaldehyde while glyceraldehyde is hydrogenated to glycerol, which is dehydrogenated back to glyceraldehyde. The glyceraldehyde also undergo dehydration to form pyruvaldehyde, which is then hydrogenated to propylene glycol [15]. The formed glycerol is also hydrogenated into propylene glycol and ethylene glycol, which can be further hydrogenated into alcohols (methanol, ethanol, and propanol).

3 Theoretical framework and mathematical formulation

3.1 Individual steps for the reaction and their rate equations

To develop the mathematical model using ordinary differential equations, we first need to establish stoichiometrically balanced reaction steps for the reaction network proposed in 1. The balanced reactions are given in Table 1.

For simplicity, the chemicals involved in each reaction step are renamed as X_1, X_2, X_3.... as shown in Table 2.

Taking P_H as the pressure of hydrogen gas, k_i's to be the rate constants, the stoichiometrically balanced reactions along with their reaction rates are as shown in Table 3.

Having derived balanced individual steps for the reaction and renamed the species, in the next subsection we then mathematically formulate the model.

Table 1. Balanced individual reaction steps in xylitol hydrogenolysis

Reaction Type	**Chemical Equation**
Xylitol dehydrogenation	$C_5H_{12}O_5 \rightarrow C_5H_{10}O_5 + H_2$
Hydrogenation of xylose	$C_5H_{10}O_5 + H_2 \rightarrow C_5H_{12}O_5$
Retro-aldol condensation	$C_5H_{10}O_5 \rightarrow C_2H_4O_2 + C_3H_6O_3$
Reformation of xylose	$C_2H_4O_2 + C_3H_6O_3 \rightarrow C_5H_{10}O_5$
Glycolaldehyde hydrogenation	$C_2H_4O_2 + H_2 \rightarrow C_2H_6O_2$
Ethylene glycol dehydrogenation	$C_2H_6O_2 \rightarrow C_2H_4O_2 + H_2$
Hydrogenation of glyceraldehyde	$C_3H_6O_3 + H_2 \rightarrow C_3H_8O_3$
Dehydrogenation of glycerol	$C_3H_8O_3 \rightarrow C_3H_6O_3 + H_2$
Glyceraldehyde dehydration	$C_3H_6O_3 \rightarrow C_3H_4O_2 + H_2O$
Pyruvaldehyde hydrogenation	$C_3H_4O_2 + 2H_2 \rightarrow C_3H_8O_2$
Glycerol to propylene glycol	$C_3H_8O_3 + H_2 \rightarrow C_3H_8O_2 + H_2O$
Glycerol to ethylene glycol	$C_3H_8O_3 + H_2 \rightarrow C_2H_6O_2 + CH_3OH$
Ethylene glycol to ethanol	$C_2H_6O_2 + H_2 \rightarrow C_2H_5OH + H_2O$
Ethylene glycol to methanol	$C_2H_6O_2 + H_2 \rightarrow 2CH_3OH$
Propylene glycol to propanol	$C_3H_8O_2 + H_2 \rightarrow C_3H_7OH + H_2O$

Table 2. Mathematical notations of the reacting species

Chemical name	Chemical formula	Mathematical notation
Xylitol	$C_5H_{12}O_5$	X_1
Xylose	$C_5H_{10}O_5$	X_2
Glycolaldehyde	$C_2H_4O_2$	X_3
Glyceraldehyde	$C_3H_6O_3$	X_4
Ethylene glycol	$C_2H_6O_2$	X_5
Glycerol	$C_3H_8O_3$	X_6
Pyruvaldehyde	$C_3H_4O_2$	X_7
Propylene glycol	$C_3H_8O_2$	X_8
Methanol	CH_3OH	X_9
Ethanol	C_2H_5OH	X_{10}
Propanol	C_3H_7OH	X_{11}

Table 3. Reaction Scheme and Rate Expressions

Reaction	**Rate Expression**
$X_1 \xrightarrow{k_1} X_2 + H_2$	Rate $= k_1 X_1$
$X_2 + H_2 \xrightarrow{k_{-1}} X_1$	Rate $= k_{-1} X_2 P_H$
$X_2 \xrightarrow{k_2} X_3 + X_4$	Rate $= k_2 X_2$
$X_3 + X_4 \xrightarrow{k_{-2}} X_2$	Rate $= k_{-2} X_3 X_4$
$X_3 + H_2 \xrightarrow{k_3} X_5$	Rate $= k_3 X_3 P_H$
$X_5 \xrightarrow{k_{-3}} X_3 + H_2$	Rate $= k_{-3} X_5$
$X_4 + H_2 \xrightarrow{k_4} X_6$	Rate $= k_4 X_4 P_H$
$X_6 \xrightarrow{k_{-4}} X_4 + H_2$	Rate $= k_{-4} X_6$
$X_4 \xrightarrow{k_5} X_7 + H_2O$	Rate $= k_5 X_4$
$X_7 + 2H_2 \xrightarrow{k_6} X_8$	Rate $= k_6 X_7 P_H^2$
$X_6 + H_2 \xrightarrow{k_7} X_8 + H_2O$	Rate $= k_7 X_6 P_H$
$X_6 + H_2 \xrightarrow{k_8} X_5 + X_9$	Rate $= k_8 X_6 P_H$
$X_5 + H_2 \xrightarrow{k_9} X_{10} + H_2O$	Rate $= k_9 X_5 P_H$
$X_8 + H_2 \xrightarrow{k_{10}} X_{11} + H_2O$	Rate $= k_{10} X_8 P_H$
$X_5 + H_2 \xrightarrow{k_{11}} 2X_9$	Rate $= k_{11} X_5 P_H$

4 The mathematical model and its basic properties

This section presents the formulation of the mathematical model. It begins with a discussion of the assumptions adopted and their justification, followed by the resulting system of ordinary differential equations, the initial conditions and the parameter estimation methods used.

4.1 Model assumptions, their justification and implications

It is assumed that the catalyst´s concentration and the hydrogen pressure are nonzero constants. These assumptions are necessary to make since they simplify the kinetic model by reducing the number of variables. They also help to focus on the core mechanism of the reaction by isolating the intrinsic kinetics of the reaction and help to simplify calculations and analysis.

However, while these assumptions simplify the kinetic analysis of the model, they also limit the applicability of the model. In industrial systems, hydrogen supply can fluctuate and catalyst concentration may change due to factors like fouling and poisoning [20]. In a study done by [3], it was revealed that mass transport effects strongly impact the activity and selectivity of catalysts in hydrogenation reactions. While the present work utilizes these assumptions to establish the kinetic framework for xylitol hydrogenolysis, future studies will build upon this foundation by adding some of these kinetics.

The formulated system includes all the reactions that have been proposed in Figure 1, a key component that has been excluded in previous literature, where these reactions were excluded by having a generalized reaction scheme for the entire mechanism.

4.2 Derivation of ODEs from the reaction mechanism

Once we have the stoichiometrically balanced equations, and assuming that the law of mass action holds for this reaction network, a system of differential equations can then be derived and they take the form:

$$\begin{cases} \frac{dX_1}{dt} &= -k_1X_1 + k_{-1}X_2P_H \\ \frac{dX_2}{dt} &= k_1X_1 - k_{-1}X_2P_H - k_2X_2 + k_{-2}X_3X_4 \\ \frac{dX_3}{dt} &= k_2X_2 - k_{-2}X_3X_4 - k_3X_3P_H + k_{-3}X_5 \\ \frac{dX_4}{dt} &= k_2X_2 - k_{-2}X_3X_4 - k_4X_4P_H + k_{-4}X_6 - k_5X_4 \\ \frac{dX_5}{dt} &= k_3X_3P_H - k_{-3}X_5 + k_8X_6P_H - k_9X_5P_H - k_{11}X_5P_H \\ \frac{dX_6}{dt} &= k_4X_4P_H - k_{-4}X_6 - k_7X_6P_H - k_8X_6P_H \\ \frac{dX_7}{dt} &= k_5X_4 - k_6X_7P_H^2 \\ \frac{dX_8}{dt} &= k_6X_7P_H^2 + k_7X_6P_H - k_{10}X_8P_H \\ \frac{dX_9}{dt} &= 2k_{11}X_5P_H + k_8X_6P_H \\ \frac{dX_{10}}{dt} &= k_9X_5P_H \\ \frac{dX_{11}}{dt} &= k_{10}X_8P_H \end{cases} \tag{1}$$

4.3 Initial conditions

At the initial time $t = 0$, the concentration for the reacting species is zero except for that of xylitol and the hydrogen pressure. In essence, we have;

$$(X_1, X_2, X_3, X_4, X_5, X_6, X_7, X_8, X_9, X_{10}, X_{11})(0) = (X_1(0), 0, 0, \ldots, 0, 0), \quad P_H > 0 \tag{2}$$

4.4 Parameter estimation and data fitting

The reaction rate constants were estimated using the numerical optimization approach and the experimental data from a laboratory report by [8]. This method combines kinetic modeling and nonlinear least-squares fitting to match experimental data.The estimated rate constants are shown in Table 4.

Table 4. Estimated rate constants presented with their orders of magnitude obtained using experimental data

Parameter	Estimated value
k_1	$\leq 10^{-2}$
k_{-1}	$\leq 10^{-2}$
k_2	$\leq 10^{1}$
k_{-2}	$\leq 10^{-1}$
k_3	$\leq 10^{-1}$
k_{-3}	$\leq 10^{-2}$
k_4	$\leq 10^{1}$
k_{-4}	$\leq 10^{-5}$
k_5	$\leq 10^{-4}$
k_6	$\leq 10^{2}$
k_7	$\leq 10^{-2}$
k_8	$\leq 10^{-6}$
k_9	$\leq 10^{-5}$
k_{10}	$\leq 10^{-7}$
k_{11}	$\leq 10^{-2}$

The fitted model was validated by comparing its predictions to experimental data (for Ni/Al_2O_3 and Ni/MgO catalysts) using weighted least squares optimization with differential evolution. For each subplot, Root Mean Squared Error (RMSE) values are shown. In both scenarios, the fitting showed good agreement with major products (propylene glycol and ethylene glycol) with RMSE < 0.1 as shown in Figures 2 and 3.

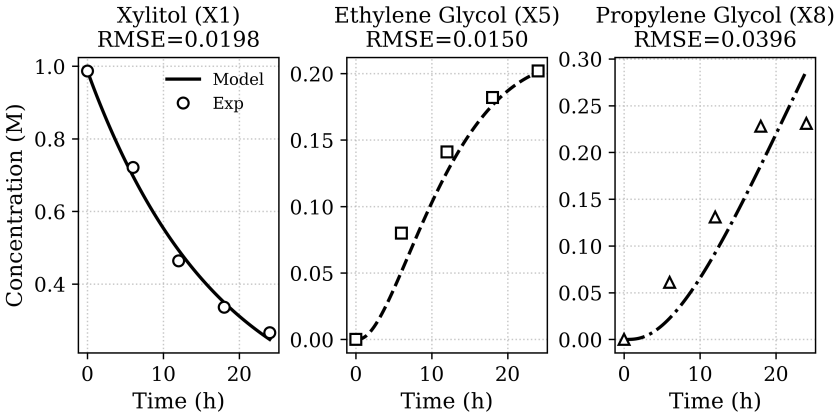

Figure 2. Comparison of model predictions and experimental data for xylitol hydrogenolysis over Ni/Al_2O_3 catalyst at 240^0C and 40 bar H_2 pressure.

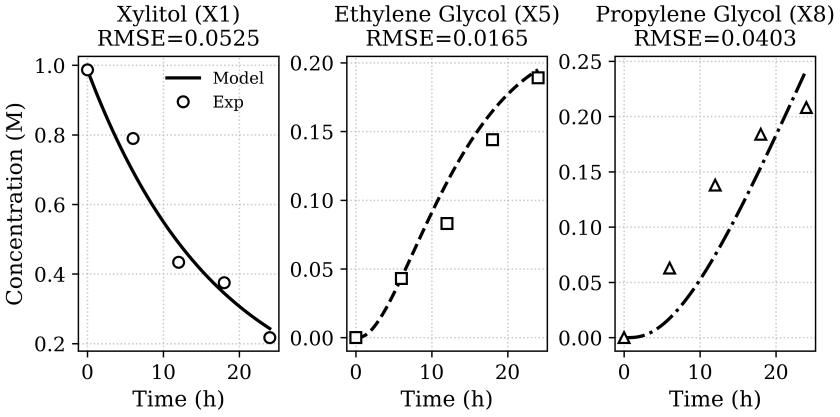

Figure 3. Comparison of model predictions and experimental data for xylitol hydrogenolysis over Ni/MgO catalyst at 240^0C and 40 bar H_2 pressure.

5 Mathematical analysis

In this section we explore the applications of qualitative analysis techniques to the model (1), with the aim of characterizing its dynamical properties and uncovering fundamental insights about the chemistry from the mathe-

matical behavior of the model. The analysis begins with an examination of the general properties and equilibria of the model, followed by a stability analysis using qualitative theory methods.

5.1 General properties of solutions

Model (1) is a system of eleven ordinary differential equations for the time evolution of the concentrations of the chemical species represented by the functions $X_i = X_i(t)$, defined in Table 3.1. Considering the case where the Hydrogen pressure P_H is kept constant, three of the 11 equations are non-linear due to the presence of the term X_3X_4 in the vector field on the right-hand side of (1). This feature prevents explicit resolution of the system (1) and thus the behavior of its solutions must be studied with an appeal to qualitative theory and numerical methods.

The right-hand side of (1) is a polynomial vector field, therefore it is C^∞, and thus locally Lipschitz. As a result, by the Picard-Lindelöf theorem one can immediately conclude that all initial value problems for (1) have a unique local (in time) solution.

From a chemical point of view, it is natural to expect that, given any non-negative initial condition $X(0) = (X_k(0))$, the solutions are nonnegative and bounded. This will be established in the next two results.

Proposition 1. *Solutions to the system in* (1) *with nonnegative initial data* $(X_k(0))$ *are nonnegative.*

Proof. We need to prove that the positive cone of $\mathbb{R}^{11}$, defined by

$$\mathbb{R}^{11^+} = \{(X_1, \ldots, X_{11}) : X_k \geq 0, \forall k\},$$

is positively invariant for the flow generated by (1). In order to prove this, it is sufficient to prove that if an initial condition is on $\partial\mathbb{R}^{11}$, then the corresponding solution $(X_k(t))$ stays in $\mathbb{R}^{11+}$ for all later times t.

Take an initial condition in $\partial\mathbb{R}^{11}$, say,

$$X_1 = 0 \bigwedge X_k > 0, \forall k = 2, \ldots, 11$$

At $t = 0$, $X_1(0) = 0, X_k(0) > 0, \forall k = 2, \ldots, 11$. From (1), we have that at $t = 0$,

$$\frac{dX_1}{dt} = -k_1 X_1(0) + k_{-1} X_2(0) P_H = 0 + k_{-1} X_2(0) P_H > 0$$

Since $X_1(0) = 0$ we can conclude from this and standard results about the relation between monotonicity and the sign of the derivative of a continuously differentiable function that $X_1(t) > 0$ for all $t > 0$ sufficiently small.

The same type of argument can be applied to initial conditions in the other planes of $\partial\mathbb{R}^{11}$, working, for each case, with an appropriate equation of the system (1) to conclude that the component that is initially equal to zero becomes strictly positive immediately afterwards:

Taking another initial condition in $\mathbb{R}^{11^+}$ as shown above, say

$$X_2 = 0 \bigwedge X_k > 0 \text{ as shown above,}$$

Then, at $t = 0$;

$$\frac{dX_2}{dt} = k_1 X_1(0) + k_{-2} X_3(0) X_4(0) > 0.$$

Therefore, $X_2(t) > 0, t > 0$.

Taking $X_3 = 0$ in $\mathbb{R}^{11^+}$, then at $t = 0$, we have;

$$\frac{dX_3}{dt} = k_2 X_2(0) + k_{-3} X_5(0) > 0, \text{ therefore } X_3(t) > 0 \text{ at } t > 0.$$

Continuing in this way, we take $X_4 = 0$ at $t = 0$, we have;

$$\frac{dX_4}{dt} = k_2 X_2(0) + k_{-4} X_6(0) > 0, \text{ therefore } X_4(t) > 0 \text{ for } t > 0.$$

With $X_5 = 0$, in $\mathbb{R}^{11^+}$ at $t = 0$ it follows that;

$$\frac{dX_5}{dt} = k_3 X_3(0) P_H + k_8 X_6(0) P_H > 0, \text{ therefore } X_5(t) > 0 \text{ at } t > 0.$$

Since $X_5(t) > 0$, from (1) it follows that

$$\frac{dX_9}{dt} > 0 \text{ and } \frac{dX_{10}}{dt} > 0.$$

As a result, $X_9(t) > 0$ and $X_{10}(t) > 0$ for $t > 0$.

Taking $X_6 = 0$ in $\mathbb{R}^{11^+}$, then at $t = 0$, we have;

$$\frac{dX_6}{dt} = k_4 X_4(0) > 0, \text{ therefore } X_6(t) > 0 \text{ for } t > 0.$$

For $X_7 = 0$, at $t = 0$, it follows that

$$\frac{dX_7}{dt} = k_5 X_4(0) > 0, \text{ therefore } X_7(t) > 0 \text{ for } t > 0.$$

Lastly, taking $X_8 = 0$ in $\mathbb{R}^{11^+}$, then at $t = 0$, we have;

$$\frac{dX_8}{dt} = k_6 X_7(0) P_H^2 + k_7 X_6(0) P_H > 0, \text{ therefore } X_8(t) > 0 \text{ for } t > 0.$$

Therefore, we can conclude that the vector field of the system (1) in $\partial\mathbb{R}^{11+}$ points inward to $\mathbb{R}^{11+}$. Then, solutions to initial value problems with nonnegative initial data cannot leave the positive cone $\mathbb{R}^{11+}$ for $t > 0$, proving the result. ■

Proposition 2. *Nonnegative solutions to* (1) *are globally defined and bounded.*

Proof. The proof is based on the conservation of mass applied to the Carbon element in all the chemical species in the system. If the molecule j has concentration X_j and contains $\hat{\jmath}$ Carbon atoms, then the total amount of Carbon in the system carried by these molecules is $\hat{\jmath} X_j$. Thus, the total amount of Carbon in the system is proportional to

$$W(X) := \sum_{j=1}^{11} \hat{\jmath} X_j, \tag{3}$$

where the values of $\hat{\jmath}$ can be easily obtained from Table 2 as $\hat{1} = 5, \hat{2} = 5, \hat{3} = 2, \hat{4} = 2$, and so on. We expect that, being $X(t)$ a solution of the differential equation system (1), the quantity of Carbon in the system is

constant with time, which means that $\frac{dW}{dt}(X(t)) = 0$. This is indeed easy to check, as we show next (to simplify notation we use $(\cdot)' := \frac{d}{dt}$):

$$
\begin{aligned}
\frac{dW}{dt} &= \frac{d}{dt}\sum_{j=1}^{11}\hat{\jmath}X_j \;=\; \sum_{j=1}^{11}\hat{\jmath}X_j' \\
&= 5X_1' + 5X_2' + 2X_3' + 3X_4' + 2X_5' + 3X_6' + 3X_7' + 3X_8' + X_9' \\
&\quad + 2X_{10}' + 3X_{11}' \\
&= \quad 5(-k_1X_1 + k_{-1}X_2P_H) \\
&\quad + 5(k_1X_1 - k_{-1}X_2P_H - k_2X_2 + k_{-2}X_3X_4) \\
&\quad + 2(k_2X_2 - k_{-2}X_3X_4 - k_3X_3P_H + k_{-3}X_5) \\
&\quad + 3(k_2X_2 - k_{-2}X_3X_4 - k_4X_4P_H + k_{-4}X_6 - k_5X_4 \\
&\quad + 2(k_3X_3P_H - k_{-3}X_5 + k_8X_6P_H - k_9X_5P_H - k_{11}X_5P_H) \\
&\quad + 3(k_4X_4P_H - k_{-4}X_6 - k_7X_6P_H - k_8X_6P_H) \\
&\quad + 3(k_5X_4 - k_6X_7P_H^2) \\
&\quad + 3(k_6X_7P_H^2 + k_7X_6P_H - k_{10}X_8P_H) \\
&\quad + (2k_{11}X_5P_H + k_8X_6P_H) \\
&\quad + 2k_9X_5P_H \\
&\quad + 3k_{10}X_8P_H \\
&= 0
\end{aligned}
$$

Hence, for all t we have $W(X(t)) = W(X(0))$, and by, the definition (3) of W, we conclude immediately that all functions $X(t)$ solving this equation in $\mathbb{R}^{11+}$ must be bounded: if one of the components $X_\ell(t)$ is not bounded then, since all $\hat{\jmath} > 0$, we would have $W(X(t)) \geq \hat{\ell}X_\ell(t)$ also unbounded, and so could not be always equal to the (bounded!) constant $W(X(0))$.

From the boundedness argument above we conclude that solutions of system (1) cannot blow to infinity in finite time and since the right-hand side of system (1) is a polynomial function, this implies that all its solutions are defined for all values of time $t \in \mathbb{R}$, [16, Corollary 3.5]. This proves the proposition. ■

5.2 Long-time behavior of solutions

In this section we study the behavior of solutions to (1) when $t \to +\infty$. For this we use the technique of Lyapunov functions.

A Lyapunov function $V : \mathbb{R}^d \to \mathbb{R}$ for a differential equation in a set $\Omega \subset \mathbb{R}^d$ is a function bounded below in Ω such that, when computed on solutions $X(t)$ of the differential equation, is non-increasing with t, which means that $\frac{dV}{dt}(X(t)) \leq 0$.

Proposition 3. *Let $X(t)$ be any non-negative solution of system (1). Then, when $t \to +\infty$, the limit of $X(t)$ exists and is a point in $\widetilde{E}_\infty := \{X \in \mathbb{R}^{11+} \,|X_j = 0,\, j = 1, \ldots, 8\}$.*

Proof. The reaction pathways presented in Figure 1 suggests that in the long-time limit all chemical species will be transformed into Methanol, Ethanol, and Propanol (X_9, X_{10} and X_{11}, respectively), and the concentrations of the remaining ones will converge to zero. This chemical insight suggests that a function similar to (3) but without terms with X_9, X_{10} and X_{11} could be appropriate.

Let $V = V(X) : \mathbb{R}^{11+} \to \mathbb{R}$ be the function defined by

$$V(X) := \sum_{k=1}^{11} \alpha_k X_k,$$

with $\alpha_1 = \alpha_2 = 2$, $\alpha_9 = \alpha_{10} = \alpha_{11} = 0$, and all other $\alpha_k = 1$. For $E > 0$ consider the region defined by

$$\mathcal{E}_E := \left\{X \in \mathbb{R}^{11+} : V(X) \leq E\right\}.$$

As all α_k in the definition of V are non-negative, the set $\mathcal{E}_E$ is bounded in $\mathbb{R}^{11+}$.

Let $X(0) = X_0 \in \mathbb{R}^{11+}$ be a non-negative initial condition and let E_0 be the positive number such that $V(X_0) = E_0$. Let $\mathcal{E}_0$ be the set $\mathcal{E}_E$ corresponding to $E = E_0$. If $X(t)$ is the solution of (1) with initial condition

X_0, then, computing $\frac{dV}{dt}(X(t))$ using (1), we get

$$\begin{aligned}
\frac{dV}{dt} &= \frac{d}{dt}\sum_{k=1}^{11}\alpha_k X_k \\
&= \ 2(-k_1X_1 + k_{-1}X_2P_H) \\
&\quad + 2(k_1X_1 - k_{-1}X_2P_H - k_2X_2 + k_{-2}X_3X_4) \\
&\quad + (k_2X_2 - k_{-2}X_3X_4 - k_3X_3P_H + k_{-3}X_5) \\
&\quad + (k_2X_2 - k_{-2}X_3X_4 - k_4X_4P_H + k_{-4}X_6 - k_5X_4 \\
&\quad + (k_3X_3P_H - k_{-3}X_5 + k_8X_6P_H - k_9X_5P_H - k_{11}X_5P_H) \\
&\quad + (k_4X_4P_H - k_{-4}X_6 - k_7X_6P_H - k_8X_6P_H) \\
&\quad + (k_5X_4 - k_6X_7P_H^2) \\
&\quad + (k_6X_7P_H^2 + k_7X_6P_H - k_{10}X_8P_H) \\
&= -(k_9 + k_{11})X_5P_H - k_{10}X_6P_H \ \leq \ 0.
\end{aligned}$$

This means that, if $(X(t))$ is a solution of the differential equation system, then

$$V(X(t)) \leq V(X_0) = E_0,$$

which implies that $X(t) \in \mathcal{E}_0$ for all $t > 0$.

LaSalle's invariance principle [16, Section 8.2.2] tells us that non-negative solutions to (1) converge to the set

$$E_\infty := \{X \in \mathbb{R}^{11+} : \frac{dV}{dt} = 0\} \quad as \quad t \to +\infty.$$

From the computation above we know that

$$\frac{dV}{dt} = 0 \Leftrightarrow (k_9 + k_{11})X_5P_H + k_{10}X_6P_H = 0$$

and thus LaSalle's principle tells us that all nonnegative solutions of (1) converge to solutions with $X_5(t) = 0$ and $X_6(t) = 0$ for all t, or, in an equivalent way, the ω-limit sets of nonnegative orbits of (1) lie in the

9-dimensional plane $X_5 = 0 \wedge X_6 = 0$, that is

$$E_\infty = \{X \in \mathbb{R}^{11+} : X_5 = X_6 = 0\}.$$

Consider now a solution of (1) in this plane. Then, since $X_6(t) \equiv 0$, we get $\frac{dX_6}{dt} = 0$ for all t, and so equation $(1)_6$ implies that $X_4(t) \equiv 0$, which of course means that also $\frac{dX_4}{dt} \equiv 0$, and hence $(1)_4$ implies that $X_2(t) \equiv 0$. Thus $\frac{dX_2}{dt} = 0$ and remembering that $X_4 \equiv 0$, equation $(1)_2$ gives $X_1(t) \equiv 0$. Using $X_4 \equiv 0$ in equation $(1)_7$ we get $\frac{dX_7}{dt} = -k_6 P_H^2 X_7$ from which we conclude that, with P_H kept constant,

$$X_7(t) = X_7(t_0) e^{-k_6 P_H^2 (t-t_0)} \to 0 \quad as \quad t \to +\infty$$

Using this expression and the fact that $X_6 \equiv 0$, equation $(1)_8$ becomes

$$\frac{dX_8}{dt} = k_6 P_H^2 X_7(t) - k_{10} P_H X_8$$

and solving this differential equation (e.g., by applying the variation of constants formula) gives

$$X_8(t) = X_8(t_0) e^{-k_{10} P_H (t-t_0)} + \\ + X_7(t_0) \frac{k_6 P_H}{k_{10} - k_6 P_H} \Big(e^{-k_6 P_H^2 (t-t_0)} - e^{-k_{10} P_H (t-t_0)} \Big),$$

from which it immediately follows that $X_8(t) \to 0$ as $t \to +\infty$. Finally, using $X_5 \equiv 0$ and $X_6 \equiv 0$ in $(1)_5$ we conclude that $X_3 \equiv 0$.

Thus, we conclude that all solutions of (1) in the set

$$E_\infty = \{X \in \mathbb{R}^{11+} : X_5 = X_6 = 0\}$$

must converge to

$$\widetilde{E}_\infty := \{X \in \mathbb{R}^{11+} : X_k = 0, \text{ for } k = 1, \ldots, 8\}$$

Furthermore, from the last three equations in (1) and the non-negativity of solutions we know that $X_9(t), X_{10}(t)$ and $X_{11}(t)$ are monotonically non-decreasing. From Proposition 2 we know that they are bounded. Hence, each of the functions $X_j(t)$, $j = 9, 10, 11$, is convergent to some $X_j^* > 0$ when $t \to +\infty$.

Thus, we proved that for every non-negative solution $X(t)$ of (1), there exists a point $X^* \in \widetilde{E}_\infty$, dependent of the initial condition and the coefficients of the system, such that, when $t \to +\infty$, $X(t) \to X^*$. This proves the result. ■

Recalling that the ω-limit set of an equilibrium solution is the solution itself, the following corollary is obvious.

Corollary 1. *All nonnegative equilibria of* (1) *are points of* $\widetilde{E}_\infty$.

It is immediate to conclude directly by inspection of (1) that if X is a point on $\widetilde{E}_\infty$ then it is an equilibrium point of the system, which is the reciprocal of Corollary 1. Thus, we proved the following result.

Proposition 4. *A point* $X^* \in \mathbb{R}^{11+}$ *is an equilibrium of* (1) *if and only if* $X^* \in \widetilde{E}_\infty$.

Actually, using the function W in the proof of Proposition 2, which we proved that it is a conserved quantity of system (1), i.e., $W(X(t)) = W(X(0))$, and taking limits as $t \to +\infty$ in this equality we conclude that the limit point of the solution $X(t)$ with initial value $X(0)$ satisfies $W(X^*) = W(X(0))$. From the above computations this means that, for an initial condition $X(0) = (X_1(0), 0, \ldots, 0)$, we must have

$$X_9^* + 2X_{10}^* + 3X_{11}^* = 5X_1(0).$$

Diagrammatically, we can show in Figure 4 the limit point of 1 which is indeed in $\widetilde{E}_\infty$. This proves the following result.

Proposition 5. *Let* $X(t)$ *be the solution of system* (1) *with an initial condition* $X(0) = (X_1(0), 0, \ldots, 0)$ *and let* $X^* = \lim_{t \to +\infty} X(t)$. *Then*

$$X_9^* + 2X_{10}^* + 3X_{11}^* = 5X_1(0). \tag{4}$$

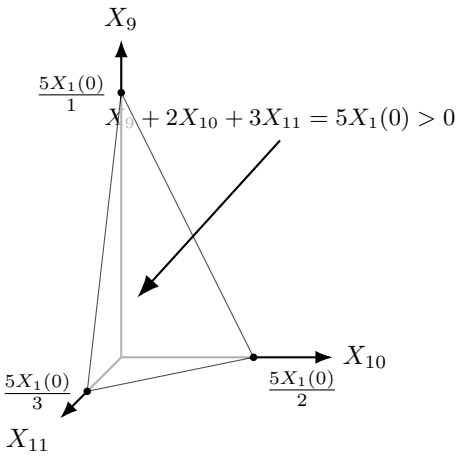

Figure 4. Pictorial illustration of the limit plane of $X_9+2X_{10}+3X_{11} = 5X_1(0) > 0$

Additional information on the precise location of the limit point X^* of a solution $X(t)$ when $t \to +\infty$ can be extremely difficult to obtain analytically [4], and in this case, with a reaction network with the complexity shown in Figure 1, it is most likely beyond what can be obtained. So, to this end, some numerical experiments are useful and will be presented in the next section.

6 Results

In this section, experimental results as well as model simulation results are presented. For the model simulation results, we first show simulations of up to 72 hrs at different ratios of xylitol to hydrogen to ascertain at which ratio do we get maximum yields of the main products. Then, we present simulations at that ratio for longer time durations.

6.1 Experimental results

The results of laboratory experiments on hydrogenolysis of xylitol using Ni/Al_2O_3 and Ni/MgO catalysts are presented in Figure 5. The results were obtained through laboratory analysis, where product concentrations

were measured at various time intervals using gas chromatography. The recorded data highlight the main products, while the minor products are classified into "others" and "alcohols".

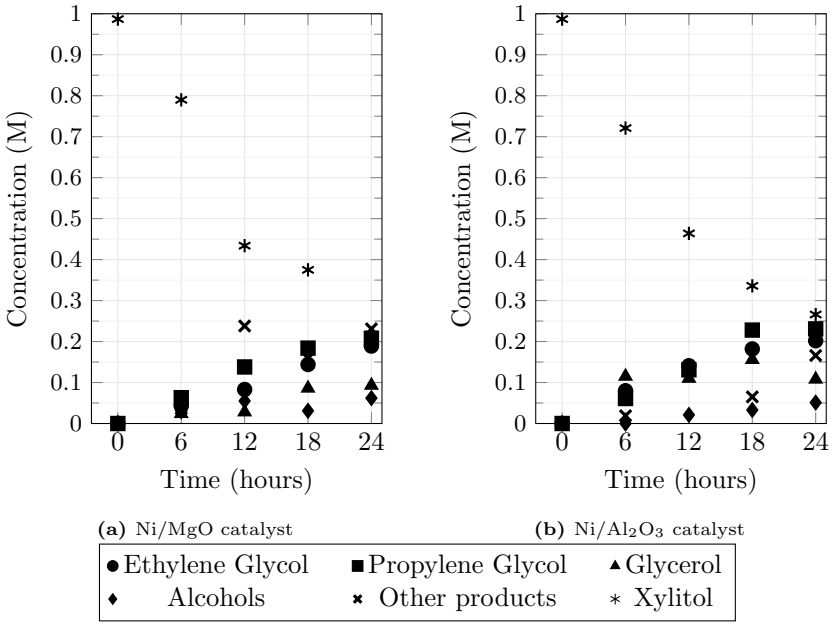

Figure 5. Experimental results for Xylitol hydrogenolysis over different Ni-based catalysts. Reaction conditions; 15% aqeous xylitol solution, 30g; catalyst mass, 0.5g; H_2 pressure , 40 bar; temperature, 240 ^0C. "Alcohols"= methanol, ethanol and propanol. "Others" = xylose, glycolaldehyde, glyceraldehyde and pyruvaldehyde

The experimental results show the dominance of propylene glycol over ethylene glycol in both catalysts. The Ni/Al_2O_3 catalyst shows an increased production of glycerol compared to Ni/MgO catalysts, and the "Others" and "Alcohols" exhibit fluctuations throughout the reaction.

6.2 Kinetic model simulation results

In this section we present the simulation results of the kinetic model performed at different hydrogen : xylitol ratios and the reaction profiles were generated and plotted computationally using Python.

The concentration values in our model were derived from experimental parameters of 15 % wt xylitol, 40 bar hydrogen pressure and at 240^0C .

Table 5 shows the values of the rate constants used for the model simulations at the different hydrogen : xylitol ratios.

Table 5. Parameter values

Parameter	Value
k_1	10^{-1}
k_{-1}	10^{-2}
k_2	10^{0}
k_{-2}	10^{-1}
k_3	10^{-1}
k_{-3}	10^{-2}
k_4	0.5
k_{-4}	10^{-2}
k_5	10^{-3}
k_6	10^{1}
k_7	10^{-1}
k_8	10^{-4}
k_9	10^{-3}
k_{10}	10^{-3}
k_{11}	10^{-3}

6.2.1 Model simulations at fixed xylitol concentrations

We first present the model results at fixed xylitol for a duration of 72 hours, as shown in Figure 6.

In Figure 7, we show the concentration profiles generated by the kinetic model by varying the amount of hydrogen while keeping xylitol fixed at longer time frames.

The results show that increasing the pressure of hydrogen while keeping the concentration of xylitol fixed shows an increase in the xylitol conversion rate and the amount of glycols that are being produced. In the H_2 : xylitol ratio of 0.5 : 1 the conversion of xylitol is slow and there is gradual formation of the intermediates as compared to the ratio of 1 : 1. A similar trend is observed when comparing glycol yields between the ratios 2 : 1 and

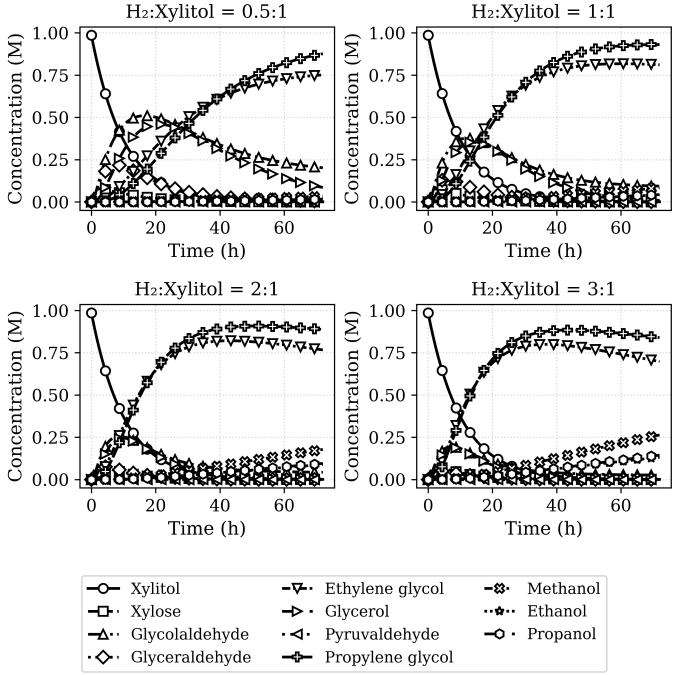

Figure 6. Simulated concentration profiles of xylitol hydrogenolysis at fixed xylitol and varying H_2 concentrations for 72 hrs. Initial conditions: 0.99M Xylitol, 40 bar H_2, Temperature= 240^0C

3 : 1. It can also be seen from the model results that at higher hydrogen pressures, the xylitol conversion rate is increased, and as a result, the time taken to give the products is less when compared to lower hydrogen pressures.

The results further show that, at higher hydrogen pressure, the production of alcohols increases. Methanol is produced in higher amounts alongside propanol compared to ethanol. When the reaction is conducted for much longer time lengths, the results show that the production of the glycols stops and only the alcohols get produced. However, the model results reveal that, even though the production of glycerol increases at higher hydrogen pressures, the total amount that is produced is relatively low as compared to the amounts of propylene glycol and ethylene glycol.

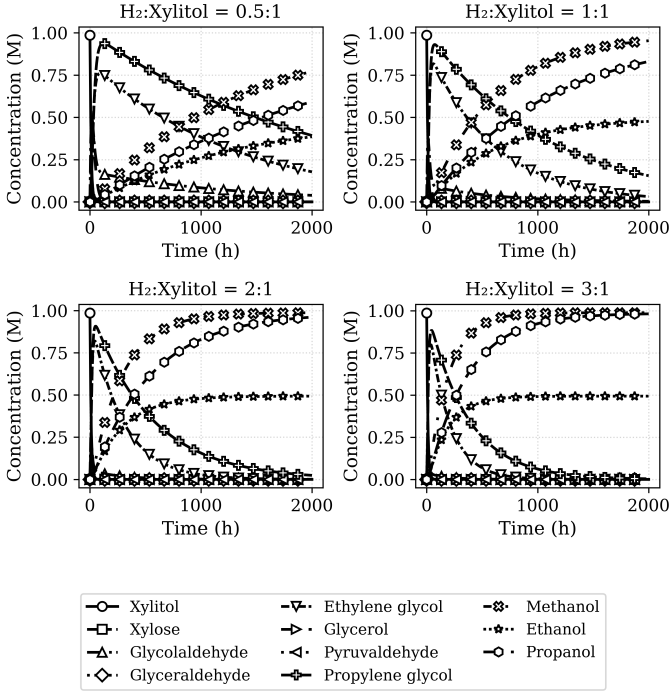

Figure 7. Simulated concentration profiles of xylitol hydrogenolysis at fixed xylitol and varying H_2 concentrations for longer t frames. Initial conditions:0.99M Xylitol, 40 bar H_2, Temperature= 240^0C

In the next subsection, we present the simulation results of the model when hydrogen is kept constant while xylitol is varied.

6.2.2 Model simulations at fixed hydrogen concentrations

The simulation results of the model in Figure 8 show that increasing the concentration of xylitol while fixing hydrogen increases the amount of propylene and ethylene glycol produced, as well as the amount of alcohols produced. The results also show that, at higher concentrations of xylitol, the production of alcohols and glycols is relatively high. Allowing the reaction to proceed for a much longer time, the results show that at higher xylitol concentrations, the production of ethylene and propylene

glycol stops and only the alcohols get produced shown in Figure 8.

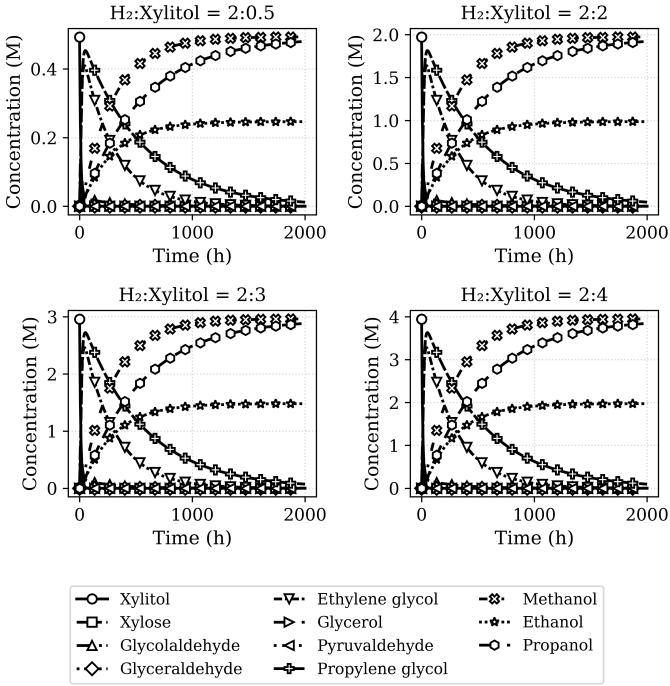

Figure 8. Simulated concentration profiles of xylitol hydrogenolysis at fixed hydrogen and varying xylitol concentrations for longer t frames. Initial conditions:0.99M Xylitol, 40 bar H_2, Temperature= 240^0C

In general, the results show that increasing the amount of xylitol while keeping the hydrogen fixed increases the amount of glycols and alcohols that are produced. However, the time taken to yield the maximum amounts of the glycols is the same at all the different ratios as shown in the next section on trend analysis.

6.2.3 Trend analysis results at fixed xylitol concentrations.

In Table 6, we present the analysis of the trend of the key products in various fixed ratios of xylitol. For each species, we report both the maximum concentration achieved and the time required to reach this maximum concentration.

Table 6. Trend analysis of the key products across fixed xylitol ratios

H_2 : Xyl	Time (h) to Maximum [EG]	$[EG]$ (M)	Time (h) to Maximum [PG]	$[PG]$ (M)
0.5 : 1	92.2	0.762	124.2	0.937
1 : 1	60.1	0.817	72.1	0.931
2 : 1	44.1	0.820	52.1	0.908
3 : 1	36.1	0.799	44.1	0.884

We then present a trend analysis of the key products across different fixed hydrogen concentrations.

Table 7. Trend analysis of the key products across fixed hydrogen ratios

H_2 : Xyl	Time (h) to Maximum [EG]	$[EG]$ (M)	Time (h) to Maximum [PG]	$[PG]$ (M)
2 : 0.5	44.1	0.410	52.1	0.454
2 : 1	44.1	1.641	52.1	1.816
2 : 3	44.1	2.461	52.1	2.723
2 : 4	44.1	3.282	52.1	3.631

6.3 Quantitative results of kinetic model against experimental results

In this section we present results on how well the model replicates experimental trends specifically for xylitol depletion, propylene and ethylene glycol formations for each catalyst. When fitting the model to the experimental data for only the production of propylene and ethylene glycol as shown in Figures 9 and 10, the following optimized rate parameters were obtained.

Table 8. Optimized Parameter values

Parameter	Value
k_1	0.058
k_{-1}	0.000063
k_2	10
k_{-2}	0.0001
k_3	0.066
k_{-3}	0.001
k_4	1.0
k_{-4}	0.00001
k_5	0.001
k_6	100
k_7	0.027
k_8	0.001
k_9	0.001
k_{10}	0.001
k_{11}	0.001

For the Ni/Al_2O_3 based catalyst, the following results were obtained along with the RMSE for each subplot.

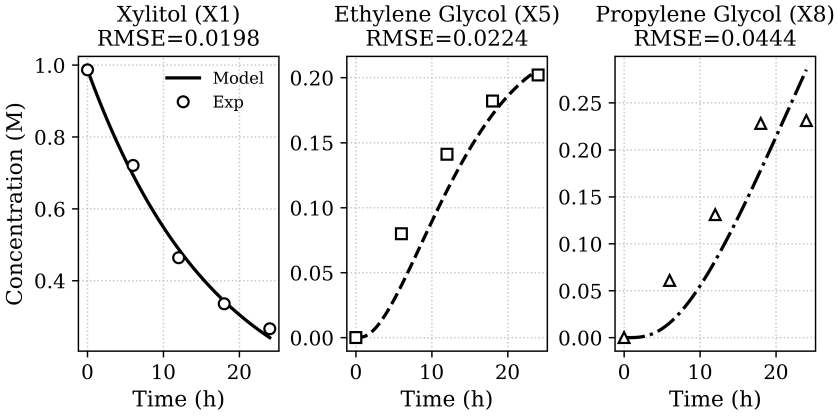

Figure 9. Experimental vs. modeled concentration profiles for xylitol hydrogenolysis over Ni/Al_2O_3 (0–25 hours)

When the model predictions were compared with the experimental results obtained using Ni/MgO based catalyst, the following results were obtained.

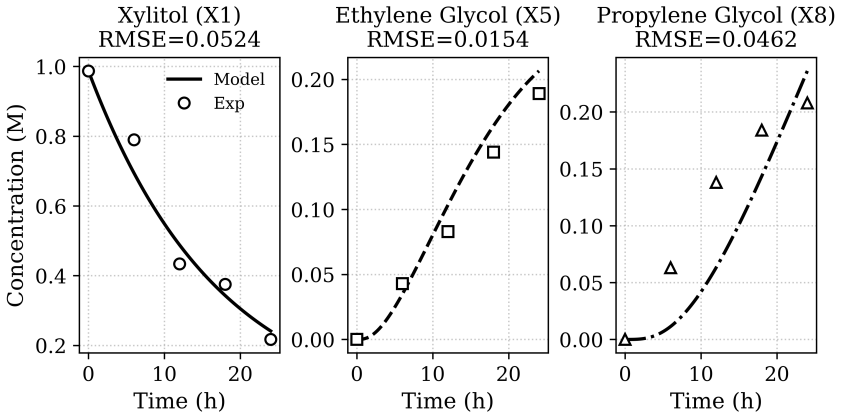

Figure 10. Experimental vs. modeled concentration profiles for xylitol hydrogenolysis over Ni/MgO (0–25 hours)

7 Discussion of results

In this section we present the discussions of the results together with the key findings as well as mechanistic insights of the model. We further highlight on the model´s limitations and areas that needs to be explored for future work.

7.1 Experimental results analysis

The experimental results as shown in Table 5 shows the dominance of propylene glycol over ethylene glycol in both catalysts. These suggests the preference of the C-C cleavage at certain specific positions in xylitol. The experimental results also shows that the production of glycerol remains relatively low in the reaction suggesting that it either gets converted into other products very fast probably due to its unstable behavior it exhibits in the Ni- based catalysts.

7.2 Mathematical results analysis

The mathematical findings of the xylitol hydrogenolysis model provides some insightful dynamics on the qualitative behaviour of the model in (1).

One of the mathematical result from the model is that its solutions exist and are unique for each value of the initial concentrations (Proposition 1). This is due to the smoothness and local Lipschitz continuity of the right handside of (1). Although uniqueness is certainly not a surprising result from the chemical point of view, it is important that mathematical models exhibit such a feature if they are going to be of any use in describing and predicting the behaviour of real systems.

The mathematical results also revealed that the positive cone $\mathbb{R}^{11+}$ is positively invariant. This means that, for any given non-negative initial conditions, the system in (1) will remain in the domain of non-negative concentrations of the chemical species. As in the result of existence and uniqueness, the mathematical model will not produce negative concentrations for these reactions.

It was also shown, mathematically that the model exhibit boundedness and mass conservation properties. This was established by showing that, based on the number carbon atoms per species, the model has a conserved function $W(X)$ and this implies that the solutions are bounded and globally defined (Proposition 2). This result guarantees that the solutions to the model do not blow up and result into non-realistic properties like infinite concentrations at longer time frames, confirming and aligning with the law of conservation of mass.

When analyzing the long-time behavior of the solutions to the model, using LaSalle's invariance principle, the results showed that solutions to the system approach a lower-dimensional invariant set;

$$\widetilde{E}_{\infty} := \{X \in \mathbb{R}^{11+} : X_k = 0, \text{ for } k = 1, \ldots, 8\}$$

From the chemistry perspective, this means that all the intermediate chemicals are converted into the alcohols; namely methanol, ethanol and propanol, as the reaction progresses, a result that is in line with the proposed reaction pathway.

Qualitatively analyzing the type of equilibria for the system showed that all the equilibria for (1) lie in the subset where only methanol, ethanol and

propanol have non-zero concentrations as shown in Proposition 4.

Having looked at the mathematical findings of our model, we then look at the simulations from the proposed kinetic model.

7.3 Model simulation analysis

The model results show that at higher H_2 concentrations, the xylitol conversion rate increases, subsequently resulting into an increase in the yields of the glycols as shown in Figure 7. The formation of methanol and propanol increases at higher H_2 concentrations, suggesting that the hydrogenation of glycols into alcohols is favored. Throughout the different ratios, the model results show that the production of glycerol remains relatively low as compared to ethylene and propylene glycol. This is in-line with the observations from the experimental results, and it suggests the transient role played by glycerol in this reaction. Therefore, when varying the amount of H_2 while fixing xylitol, the model results shows that the process favors the production of glycols due to excess hydrogenolysis , but at longer reaction times, the production of alcohols is favored, suggesting the further hydrogenolysis of the glycols into the alcohols.

Results from Figure 8 shows that an increase in xylitol concentration yields to an increase in the production of glycols as well as alcohols. The production of alcohols is dominant at longer reaction times, suggesting the conversion of the glycols into alcohols. Glycerol production still remain relatively low even at higher xylitol concentrations suggesting its minor kinetic effects in this reaction. This trend suggests that even though increasing the concentration of xylitol improves the reaction´s selectivity towards glycols, this also increase the production of alcohols, especially at longer reaction times. These then raise the need to optimize reaction with xylitol concentration to have better selectivity towards glycols.

8 Conclusions

8.1 Insights from the model

The model predicts that propylene glycol is kinetically favored over ethylene glycol and this is in consistency with the experimental results. The model further predicts that at higher H_2 concentrations, there is excess hydrogenolysis that favors the production of glycols, however, at higher values of t, alcohols production becomes dominant. This is in accordance with the use of H_2 in the industry to optimize and standardize selectivity towards glycols. The relatively low amounts of glycerol produced in the different ratios suggest that it is rapidly consumed into other products because of its instability in the catalysts, thus playing a minimal role in the kinetics of this reaction.

8.2 Limitations of current model

The kinetic model formulated for xylitol hydrogenolysis assumes constant catalyst´s concentration. In practice, catalyst deactivation strongly affects the dynamics of the reactions over time and subsequently alters the performance [20]. A more detailed microkinetic model may address these effects. The model also assumes isothermal conditions, which is not the case with real-world systems. Here, exothermic or endothermic reactions can lead to localized heating and, as a result, alter the rate of the reaction as well as the stability of the catalyst.Hence, future work might need to include energy balance terms to account for these thermal effects.

Another limitation is the simplified experimental data. The experimental data used to develop this model grouped all the intermediates as "others" and the alcohols as "alcohols". With these groupings, it means that all the intermediates and the alcohols in these reaction exhibit similar dynamics in the reaction, which is not the case, from the chemistry point of view. These then made the fitting of the model to the experimental data difficult, since the model quantifies the intermediates as well as the alcohols while the available experimental data generalized and grouped the products. Therefore, there is a need for some more detailed experimental data so to

improve the kinetic model.

Overall, the model have established a framework for kinetic modeling of complex reaction networks which can be used as a tool to optimize and maximize the yields of desired products, which is a very crucial aspect in chemical synthesis.

8.3 Recommendations

To further develop and advance the model, it is recommended that experimental data that captures the distribution of the intermediates can be used instead of the more generalized one when it comes to intermediates and alcohols. This would then allow the model to better fit into the experimental data, increasing its predictability power.

It can also be recommended that other features like mass transfer, solvent effects, catalyst decay and adsorption kinetics be included in the kinetic model to increase its prediction power. This can be achieved by using this model alongside other models which cater for these features like the Langmuir-Hinshelwood which accounts for the adsorption kinetics on the catalyst´s site [11].

Additionally, deep learning techniques such as neural networks can be incorporated into our model to improve its predictability power. This approach could be of good benefit given the limited experimental data for this reaction.

***Acknowledgment*:** The authors would like to express their sincere and heartfelt gratitude to the University of KwaZulu-Natal, particularly the Discipline of Chemistry within the School of Agriculture and Science for funding this work. FPdC is partially funded by *FCT - Fundação para a Ciência e a Tecnologia, I.P.* (Portugal), through national funds, under the project UID/04561/2025.

References

[1] M. Besson, P. Gallezot, C. Pinel, Conversion of biomass into chemicals over metal catalysts, *Chem.Rev.* **114** (2014) 1827–1870.

[2] J. J. Bozell, G. R. Petersen, Technology development for the production of biobased products from biorefinery carbohydrates—the US Department of Energy's "Top 10" revisited, *Green Chem.* **12** (2010) 539–554.

[3] O. E. B. Corstius, M. Kikkert, S. T. Roberts, E. J. Doskocil, J. E. S. van der Hoeven, P. E. de Jongh, Mass transport effects in gas-phase selective hydrogenation of 1,3-butadiene over supported Pd, *React.Chem.Eng.* **9** (2024) 1726–1738.

[4] F. P. da Costa, *A note on the selection of equilibria in some chemical reaction schemes*, unpublished note, 2019.

[5] C. Heisig, C. Glotzbach, S. Schirrmeister, T. Turek, Selective hydrogenolysis of biomass-derived xylitol to glycols, *Chem. Eng. Techn.* **44** (2021) 761–772.

[6] G. W. Huber, S. Iborra, A. Corma, Synthesis of transportation fuels from biomass: chemistry, catalysts, and engineering, *Chem. Rev.* **106** (2006) 4044–4098.

[7] B. MacQueen, M. Royko, B. S. Crandall, A. Heyden, Y. J. Pagán-Torres, J. Lauterbach, Kinetics study of the hydrodeoxygenation of xylitol over a ReOx-Pd/CeO_2 catalyst, *Catalysts* **11** (2021) #108.

[8] V. Ndabankulu, *Conversion of Xylitol to Ethylene and Propylene Glycols Using Supported Ni Catalysts: Laboratory Report*, Unpublished report, University of KwaZulu-Natal, Chemistry Laboratory, Westville Campus, 2024.

[9] Q. Ndlovu, M. Shozi, F. da Costa, Mathematical investigations of a kinetic model for glycerol hydrogenolysis, *MATCH Commun. Math. Comput. Chem.* **88** (2022) 437-460.

[10] M. Rivière, N. Perret, A. Cabiac, D. Delcroix, C. Pinel, M. Besson, Xylitol hydrogenolysis over ruthenium-based catalysts, *ChemCatChem* **9** (2017) 2145–2159.

[11] R. Smith, M. Jones, Application of Langmuir-Hinshelwood kinetics in methane reforming, *Catalysis Today* **12** (1991) 50–65.

[12] Statista Research Department. *Global ethylene glycol production capacity, 2022.*

Available at: https://www.statista.com/statistics/1067418/global-ethylene-glycol-production-capacity/ Accessed on 2024-08-29.

[13] Statista Research Department. *Global carbon dioxide emissions, 2023*. Available at: https://www.statista.com/statistics/276629/global-co2-emissions/. Accessed on 2024-08-21.

[14] Statista Research Department. *Global propylene glycol production capacity, 2023*. Available at: https://www.statista.com/statistics/276629/global-co2-emissions/. Accessed on 2024-08-21.

[15] J. Sun, H. Liu, Selective hydrogenolysis of biomass-derived xylitol to ethylene glycol and propylene glycol on supported Ru catalysts, *Green Chem.* **13** (2011) 135–142.

[16] M. Viana, J. Espinar, *Differential Equations: A Dynamical Systems Approach to Theory and Practice*, Am. Math. Soc., Providence, 2021.

[17] S. Wang, Y. Zhang, H. Liu, Selective hydrogenolysis of glycerol to propylene glycol on Cu–ZnO composite catalysts, *Chem.Asian J.* **5** (2010) 1100–1111.

[18] T. Werpy, G. Petersen, *Top Value Added Chemicals from Biomass*, U.S. Dept. Energy, Washington, 2004.

[19] Q. Xia, G. Zhang, J. Wang, W. Zhang, M. Liu, Y. Li, B. Yin, C. Yang, J. Shen, X. Jin, Synergistic bimetallic Pd–Pt/TiO_2 catalysts for hydrogenolysis of xylitol, *Ind. Eng. Chem. Res.* **59** (2020) 13879–13891.

[20] Y. Zeng, X. Han, C. C. Xu, M. Zhang, Catalyst deactivation during hydrotreating, in: M. R. Rahimpour, A. Bakhtyari, M. A. Makarem (Eds.), *Advances in Hydrotreating for Integrated Biofuel Production*, Elsevier, 2024, pp. 233–249.